Proceedings of the 28th IEEE
EMBS Annual International Conference
New York City, USA, Aug 30-Sept 3, 2006

Modeling the Nonlinear Dynamic Interactions of the Lateral and the Medial Perforant Path of the Hippocampal Dentate Gyrus

Angelika Dimoka, Spiros H. Courellis, Vasilis Z. Marmarelis, and Theodore W. Berger

Abstract—We present a new method to characterize the nonlinearities resulting from the co-activity of two pathways that converge on a common postsynaptic element. We investigated the nonlinear dynamic interactions between the Lateral Perforant Pathway (LPP) and the Medial Perforant Pathway (MPP) of the hippocampal dentate gyrus, and the effects of these cross-pathway interactions on granule cell output. A third order Volterra-Poisson modeling approach was implemented to capture the interactions between the two pathways. The kernels presented pathway specific signatures as they capture the nonlinear dynamics of each pathway individually in the form of self-kernels, and the nonlinear interactions between the two pathways in the form of cross-kernels. Data were collected in-vitro from acute slices of adult rats via a multi-electrode array recording system. The stimuli were dual-site random impulse trains with Poisson distributed inter-impulse intervals. The recorded responses from the granule cells were population spikes, simplified as discrete impulses with variable amplitudes. Our results indicated that the third order nonlinear interactions between the LPP and the MPP needs to be included in the model in order to achieve adequate predictive accuracy and indicate that this approach can be generalized to complex interactions between distinct inputs to the same set of neurons.

I. Introduction

The hippocampus is one of the most extensively studied neuronal systems aiming to advance our understanding of the mechanisms that underlie higher cognitive functions, such as learning and memory [1, 2]. It receives neuronal inputs from multiple brain regions that are involved in processing different sensory information and converge to a common population of postsynaptic neurons.

The dentate gyrus is the first hippocampal sub-region that receives the primary input of the hippocampus via the perforant path that arises from the entorhinal cortex (Fig. 1). The perforant path consists of two distinct synaptic inputs/pathways (the lateral and the medial perforant paths) that receive and integrate cognitive information (e.g., visual, auditory and olfactory) from other brain regions [3]. The lateral perforant path (LPP) and the medial perforant path (MPP) are straightforward to isolate because they are anatomically and functionally distinct [4]. Both pathways converge in a common population of neurons, the granule cells.

In this paper, we present a third order Volterra-Poisson model to characterize the functional properties of the dentate gyrus of the hippocampus [5]. In particular, we model the short-term, non-linear dynamic interactions between the LPP and the MPP. The proposed model provides a compact quantitative representation of the dentate gyrus based on experimentally available datasets [6]. It is mathematically rigorous and scalable with predictive capabilities [7]. The predictive accuracy of the proposed model is quantitatively evaluated using the normalized mean squared error. This model has the ability to represent the combined activities of all known and unknown characteristics of neuronal interactions without explicit knowledge of the underlying neuronal mechanisms. As additional aspects of neuronal mechanisms and functions are introduced it can be extended to incorporate increased complexity. The Volterra self and cross kernels are the quantitative descriptors of the system's input/output relationships that fully capture and quantify the nonlinear characteristics associated with the neuronal functional properties.

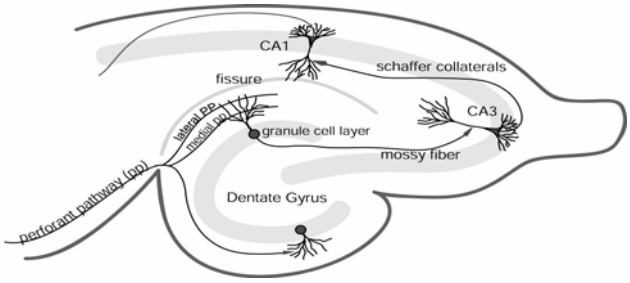

Fig. 1. Hippocampal slice circuitry.

II. Methodology

Adult Sprague-Dawley male rats were selected at the age of 7-9 weeks. Standard electrophysiological methods were used to prepare 350-400 μm thick slices and record from them [8]. Each slice was positioned over an inverted microscope (DML, DMIRB, Leika, Germany) so that the electrodes would cover the molecular layer, the fissure, and the granule cell body layer at the upper blade of the dentate gyrus. The accurate positioning of the slice (Fig. 2) was documented with a digital camera (Hitachi VK-C370, Spot Model 2.0.0).

Silicon-based, planar, multi-site electrode arrays were used to distinguish and selectively stimulate the two paths,

Manuscript received April 3, 2006. This work was supported by NSF, DARPA(HAND), and NIH(NIBIB).

A. Dimoka is with the Department of Biomedical Engineering, Center for Neural Engineering, University of Southern California, Los Angeles, CA 90089 USA (phone: 213-740-8061; fax: 213-740-0343; e-mail: dimoka@usc.edu).

S.H. Courellis is with the Department of Biomedical Engineering, University of Southern California, Los Angeles, CA 90089 USA (e-mail: shc@usc.edu).

V. Z. Marmarelis is with the Department of Biomedical Engineering, Center for Neural Engineering, University of Southern California, Los Angeles, CA 90089 USA (e-mail: vzm@bmsr.usc.edu).

T. W. Berger is with the Department of Biomedical Engineering, Program in Neuroscience, Center for Neural Engineering, University of Southern California, Los Angeles, CA 90089 USA (e-mail: berger@bmsr.usc.edu).

and to record the responses from the electrodes in the granule cell body layer. The multi-site electrode arrays were designed and fabricated so that the spatial distribution of electrode sites be appropriately arranged to cover the subregions of the molecular layer. Stimulation electrodes were chosen in the outer-molecular layer and in the mid-molecular layer to activate the LPP and MPP, respectively.

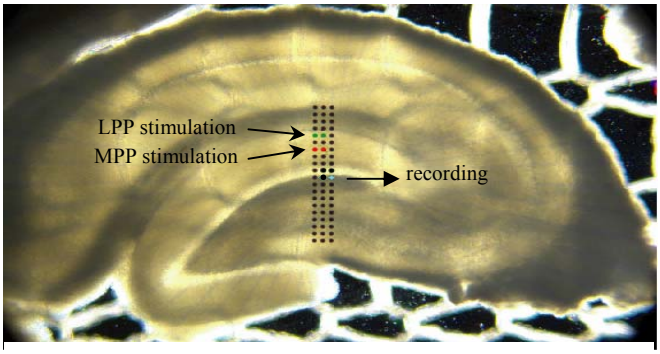

Fig. 2. Slice of the rat hippocampus positioned on the electrode array.

Stimuli sequences with 400 impulses were applied jointly to the MPP and LPP. The stimuli were independent RITs with Poisson distributed inter-impulse intervals having a mean frequency of 2Hz. The recorded responses were population spikes, simplified as discrete impulses with variable amplitudes.

Using the datasets specified above, we derived kernels based on the third order Volterra-Poisson modeling approach [9], adapted for impulse sequence stimuli and population spike responses [10]. The two inputs of the system, one in LPP and one in MPP are point processes that can be expressed for the LPP and for the MPP as:

$$x_L = \sum_{n_{j_L}} \delta(n - n_{j_L}) \quad x_M = \sum_{n_{j_M}} \delta(n - n_{j_M})$$

The population spike amplitude response recorded at the granule cell layer is:

$$y(n_i) = y_L(n_{i_L}) + y_M(n_{i_M})$$

where $y(n_i)$ is the output at discrete time n_i, the time of occurrence of the *i-th* impulse.

The population spike amplitude response attributed to the LPP input can be expressed as:

$$\begin{aligned} y_L(n_{i_L}) = k_{1y_L} &+ \sum_{n_{j_L}} k_{2y_Lx_L}(n_{i_L} - n_{j_L}) + \sum_{n_{j_M}} k_{2y_Lx_M}(n_{i_L} - n_{j_M}) + \\ &\sum_{n_{j_L}}\sum_{n_{j'_L}} k_{3y_Lx_Lx_L}(n_{i_L} - n_{j_L}, n_{i_L} - n_{j'_L}) + \\ &\sum_{n_{j_L}}\sum_{n_{j'_M}} k_{3y_Lx_Lx_M}(n_{i_L} - n_{j_L}, n_{i_L} - n_{j_M}) + \\ &\sum_{n_{j_M}}\sum_{n_{j'_M}} k_{3y_Lx_Mx_M}(n_{i_L} - n_{j_M}, n_{i_L} - n_{j'_M}) \end{aligned} \quad (1)$$

and the population spike amplitude response attributed to the MPP can be expressed as:

$$\begin{aligned} y_M(n_{i_M}) = k_{1y_M} &+ \sum_{n_{j_L}} k_{2y_Mx_L}(n_{i_M} - n_{j_L}) + \sum_{n_{j_M}} k_{2y_Mx_M}(n_{i_M} - n_{j_M}) + \\ &\sum_{n_{j_L}}\sum_{n_{j'_L}} k_{3y_Mx_Lx_L}(n_{i_M} - n_{j_L}, n_{i_M} - n_{j'_L}) + \\ &\sum_{n_{j_L}}\sum_{n_{j'_M}} k_{3y_Mx_Mx_L}(n_{i_M} - n_{j_M}, n_{i_M} - n_{j_L}) + \\ &\sum_{n_{j_M}}\sum_{n_{j'_M}} k_{3y_Lx_Mx_M}(n_{i_M} - n_{j_M}, n_{i_M} - n_{j'_M}) \end{aligned} \quad (2)$$

where n_j is the time of occurrence of any prior *j-th* impulse within the time window of μ, k_{1y_L} and k_{1y_M} are the first order kernels for the LPP and the MPP inputs respectively, $k_{2y_Lx_L}$ and $k_{2y_Mx_M}$ are the second order self-kernels, $k_{2y_Lx_M}$ and $k_{2y_Mx_L}$ are the second order cross-kernels, $k_{3y_Lx_Lx_L}$ and $k_{3y_Mx_Mx_M}$ are the third order self-kernels, and $k_{3y_Lx_Lx_M}$, $k_{3y_Lx_Mx_M}$, $k_{3y_Mx_Mx_L}$, and $k_{3y_Mx_Lx_L}$ are the third order cross-kernels. The first order kernel represents the mean of the amplitude of the population spike. The second order kernel represents the interactions between the present stimulus impulse and each of the past stimulus impulses within the memory window μ. In turn, the third order kernel represents the interaction between the present stimulus impulse and any two preceding stimulus impulses within the memory window μ. The self-kernels capture the nonlinear dynamic interactions within one pathway. The cross-kernels capture the nonlinear dynamic interactions between the two pathways. The kernels are approximated with linear combinations of exponentially decaying Laguerre functions in order to reduce the kernel estimation effort [7], which are estimated using least-squares methods [9].

The predictive accuracy of the estimated kernels was evaluated using the Normalized Mean Square Error (NMSE) to measure how well kernels can capture the system nonlinear dynamics. NMSE is defined as:

$$NMSE = \frac{\sum_i (Y_{pr_i} - Y_{data_i})^2}{\sum_i Y_{data_i}^2} \quad (3)$$

where Y_{pr} is the predicted amplitude of the population spikes using the computed kernels and Y_{data} is the recorded amplitude of the population spikes.

The descriptor widely used to characterize the two paths has been the Paired Impulse Function (PIF) [10, 11]. The measured PIF is defined as the ratio of the amplitude of the 2nd pulse over the 1st pulse resulting from stimulation with paired pulses (PP) with a given inter-pulse interval (IPI):

$$\text{measured PIF}(\Delta n) = \frac{Y_2(n_2)}{Y_1(n_1)} \quad (4)$$

where Y_1 is the amplitude of the population spike of the test response, Y_2 is the amplitude of the population spike of the conditioned response, and Δn is the IPI between the two

pulses. PIF values greater than one indicate PP facilitation, while PIF values less than one indicate PP depression.

In the context of the proposed third-order Volterra-Poisson modeling approach, the estimated self-kernels can be used to compute the conditioned response to a single input, equivalent to the one measured in the PP experiments. For instance, the conditioned response $\tilde{y}_{cond}$ for the LPP input can be computed by considering only the self-kernels of the Volterra model of Equation (1) as follows:

$$\hat{y}_{COND}(LPP) = k_{1_{y_L}} + k_{2_{y_L x_L}}(\Delta n) + k_{3_{y_L x_L x_L}}(\Delta n, \Delta n) \quad (5)$$

We can obtain the computed PÎF by dividing both sides of Equation (5) with the corresponding first order kernels:

$$\text{computed PÎF (LPP)} = 1 + \frac{k_{2_{y_L x_L}}(\Delta n) + k_{3_{y_L x_L}}(\Delta n, \Delta n)}{k_{1_{y_L}}} \quad (7)$$

Similarly the computed PÎF could be expressed for the MPP. The value of the computed PÎF is an estimate of the measured PIF for the corresponding pathway/input and will be a close approximation if, and only if, the employed third-order Volterra model is an adequate model for the subject system.

III. Results

In this study, we used 5 adult male Sprague-Dawley rats. We identified the LPP and MPP stimulation sites combining anatomical and electrophysiological criteria[8].

A third order Volterra-Poisson model adapted for the two input/one output case was used to analyze the data. For the optimum values of the Laguerre functions L and the parameter α for each dataset, the first, second and third order kernels were calculated. The mean value of the first order kernel for the LPP was 186.75 μV ± 54.9 μV and for the MPP was 276.65 μV ± 22.1 μV. The mean values of the normalized second order self and cross kernels over the corresponding first order kernels for the LPP and the MPP (Fig. 3) were calculated.

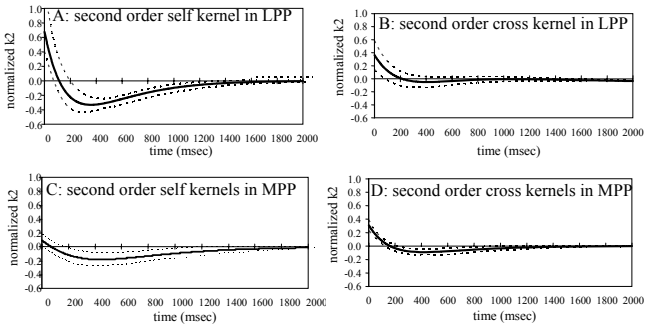

Fig. 3. The mean value of the normalized second order self kernels in LPP (A) and MPP (C). The mean value of the normalized second order cross kernels in LPP (B) and MPP (D). The dotted line shows ± one standard deviation of five different experiments.

The mean values of the normalized third order kernels ± one standard deviation are shown in Fig. 4 for LPP. Figure 4B shows the mean of the normalized third order self kernel, while Figure 4E and 4H shows the mean of the normalized third order cross kernels ($k_{3_{y_L x_L x_M}}$ and $k_{3_{y_L x_M x_M}}$).

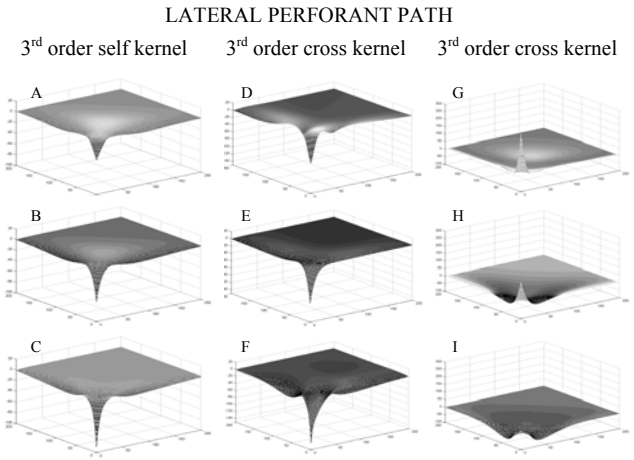

Fig. 4. The mean value of the normalized second order self (B) and cross (E, H) kernels in LPP plus (A, D, G) or minus (C, F, I) one standard deviation.

Fig. 4A, 4D and 4G show the mean of the corresponding normalized k_3 value plus one standard deviation, and Figure 4C, 4F and 4I show the mean the mean of the corresponding normalized k_3 value minus one standard deviation. The results for the MPP are show in Fig. 5.

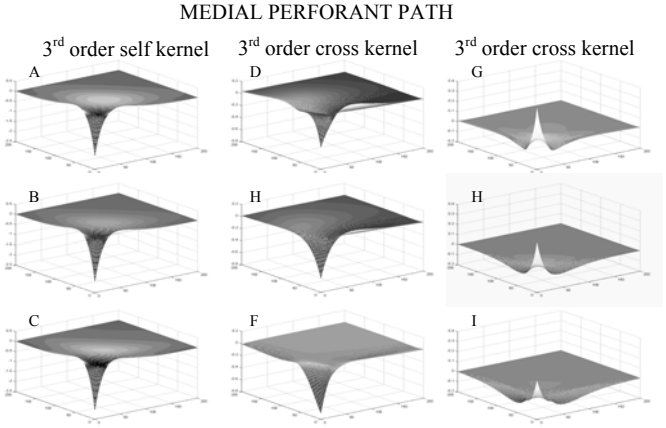

Fig. 5. The mean value of the normalized second order self (B) and cross (E, H) kernels in MPP plus (A, D, G) or minus (C, F, I) one standard deviation.

The NMSE was calculated both either including or not including the cross kernels. Using only the self kernels, the value of NMSE was 14.39±3.86%. When both the self and the cross kernels were included the NMSE dropped its value to 5.88±2.51%. The inclusion of the cross kernels improved the NMSE by 8.52%, a value that was significantly lower ($p<0.01$) than the respective NMSE value when only the self kernels were taken into account (Fig. 6).

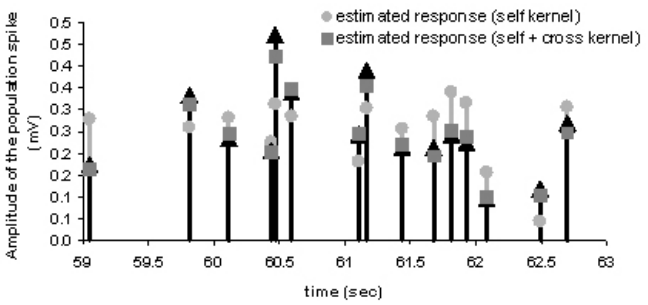

Fig. 6. System response and computed response using the third order kernel model. (▲) represent the actual response recorded through the experiment. (○) represent the estimated response using only the self kernels. (■) represent the estimated response using both the self and cross kernels.

In order to determine the ability of the proposed third-order Volterra-Poisson model to approximate the PP system dynamics, five experiments were conducted using both PP and RIT sequences. From the PP responses and Equation 4, the mean and standard deviation of the measured PIF were computed (Fig. 7A for LPP and Fig. 7B for MPP). Using the first, second and third order self-kernels, we obtained the mean and standard deviation of the computed PÎF (solid line-Fig. 7A for LPP and Fig. 7B for MPP) Figures 7A and 7B, the computed PÎF calculated from the third-order Volterra-Poisson model closely tracked the measured PIF from the PP responses. The correlation between the measured and computed PIF was statistically significant for the LPP ($p < 0.0001$) and the MPP ($p < 0.0001$).

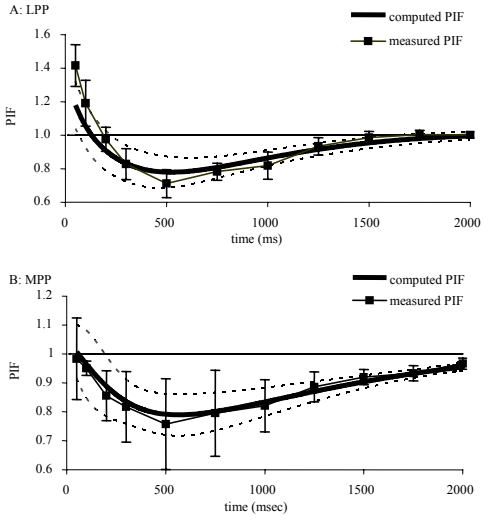

Fig. 7. System's dynamics under RIT (computed PÎF) and PP (measured PIF) in LPP (A), and in MPP (B). The dotted lines show ± one standard deviation for the RIT and the bars show the standard deviation for the PP.

These findings indicate that the third-order Volterra-Poisson model is adequate for representing the PP system dynamics.

IV. Discussion

We have presented and experimentally validated a third-order Volterra-Poisson model to describe the dynamic interactions of the LPP and the MPP of the dentate gyrus of the hippocampus. In our approach, the functional properties of the two pathways are represented as self and cross kernels that are computed using experimental data obtained by stimulating the afferents of each pathway with random impulse trains and simultaneously recording the activity of the neurons at the dentate gyrus. The proposed Volterra-Poisson model exhibited highly accurate predictive capabilities, surpassing by large any type of prediction that the traditional approach, using the measured PIF, could offer. The predictive power of the model was fully illustrated.

The third order Volterra-Poisson model presented in this paper offers a quantitative description of the functional characteristics of the dentate gyrus of the hippocampus, by fully characterizing the short-term plasticity of the LPP and the MPP. It is a predictive model with high prediction accuracy that can be used to produce responses to arbitrary input patterns. Future research will extend the model to include a quantitative representation of the interactions among hippocampal pathways. Modeling these interactions will advance our understanding of the information fusion that occurs at the dentate gyrus. The proposed modeling approach provides a methodological framework for investigating the functional properties of the hippocampus expressed at the system level and can be readily extended to model other parts of the nervous system.

References

[1] T. V. Bliss and T. Lomo, "Long-lasting potentiation of synaptic transmission in the dentate area of the anaesthetized rabbit following stimulation of the perforant path," *Journal of Physiology, London*, vol. 232, pp. 331-356, 1973.

[2] J. O'Keefe and L. Nadel, "The hippocampus as a cognitive map," *Behavioral and Brain Sciences*, vol. 2, pp. 487-533, 1979.

[3] L. Uva and M. de Curtis, "Polysynaptic olfactory pathway to the ipsi- and contralateral entorhinal cortex mediated via the hippocampus," *Neuroscience Letters*, vol. 130, pp. 249-258, 2005.

[4] A. Hjorth-Simonsen, "Projection of the lateral part of the entorhinal area to the hippocampus and fascia dentata," *J Comp Neurol*, vol. 146, pp. 219-32, 1972.

[5] V. Z. Marmarelis and T. W. Berger, "General methodology for nonlinear modeling of neural systems with Poisson point-process inputs," *Mathematical Biosciences*, vol. 196, pp. 1-13, 2005.

[6] G. Gholmieh, S. H. Courellis, A. Dimoka, J. D. Wills, J. La Coss, J. J. Granacki, V. Z. Marmarelis, and T. W. Berger, "An algorithm for real-time extraction of population EPSP and population spike amplitudes from hippocampal field potential recordings," *J Neuroscience Methods*, vol. 136, pp. 111-121, 2004.

[7] V. Z. Marmarelis, "Identification of nonlinear biological systems using Laguerre expansions of kernels.," *Annals of Biomedical Engineering*, vol. 21, pp. 573-589, 1993.

[8] A. Dimoka, S. H. Courellis, D. Song, V. Z. Marmarelis, and T. W. Berger, "Identification of the lateral and medial perforant path of the hippocampus using single and dual random impulse train stimulation," presented at Proceedings of the 25th Annual International Conference of the IEEE, 2003.

[9] S. H. Courellis, V. Marmarelis, and T. Berger, "Modeling event-driven nonlinear dynamics," presented at Biological Neural Networks, 2000.

[10] B. L. McNaughton, "Evidence for two physiologically distinct perforant pathways to the fascia dentata.," *Brain Research*, vol. 199, pp. 1-19, 1980.

[11] A. Colino and R. Malenka, "Mechanisms Underlying Induction of Long-Term Potentiation in Rat Medial and Lateral Perforant Paths In vitro," *Journal of Neurophysiology*, vol. 69, pp. 1150-1159, 1993.